Prabha Materials Science Letters
Vol. 5, No. 1, 51-73, 2026
https://doi.org/10.33889/PMSL.2026.5.1.004

Linear Instability in Hybrid Nanofluids Under Horizontal Pressure Gradient and Local Thermal Non-Equilibrium Effects

Jyoti Ahuja
Department of Mathematics,
Post Graduate Government College, Sector-11, Chandigarh, India.
E-mail: jyotiahuja@gc11.ac.in

Jyoti Sharma
University Institute of Engineering and Technology,
Panjab University, Chandigarh, India.
Corresponding author: jyoti.maths@gmail.com, sharma.jyoti@pu.ac.in

(Received on September 1, 2025; Revised on December 14, 2025; Accepted on January 8, 2026)

Abstract
The present study considers the hybrid nanofluid convection problem under the local thermal non-equilibrium (LTNE) model. A horizontal pressure gradient is applied, which influences the initial profile of the velocity of the fluid layer. Linear stability analysis is applied to find the expression of thermal Rayleigh number and found to be a function of many non-dimensional numbers introduced due to LTNE and the hybrid character of the fluid. Further, the outcome is subsequently verified and contrasted with a less intricate convection system, leading to noteworthy observations. For a thorough investigation of the problem, metallic (copper, silver) and non-metallic (alumina, titanium dioxide) nanoparticles in base fluids (water and ethylene glycol) are used for numerical computations of the problem. The effect of nanoparticles destabilizes the system in LTE cases however additional impact of LTNE tends to postpone the onset of convection significantly. The hybrid character of the system makes it less stable than mono nanofluids in the LTE case. However, this does not apply to the LTNE model, where the onset of instability depends on the various physical characteristics of the system. To understand the deep insight into the convection process, various values of parameters are calculated and presented in the tables along with stability curves for hybrid and mono nanofluids which are analysed together. The analysis reveals that increasing the base-fluid conductivity and viscosity enhances the sensitivity of the layer, whereas higher density and specific heat of the base fluid suppress convection. An increase in thermal conductivity and nanoparticle volume fraction promotes system stability, while higher particle density and specific heat act to destabilize the layer. Water acts as a more stable base fluid than ethylene glycol due to its lower viscosity, highlighting viscosity as a dominant stabilizing property. Among the nanoparticles, alumina is more stabilizing than titanium dioxide due to its higher conductivity and lower density. Copper enhances the stability of water more effectively than alumina, though the order reverses for ethylene glycol, where particle density through the concentration Rayleigh number, becomes dominant. Silver nanoparticles make the layer more sensitive than copper particles because of their higher density and thermal diffusivity ratio.

Keywords- Local thermal non-equilibrium model, Hybrid nanofluids, Linear stability analysis, Horizontal pressure gradient, Metallic and non-metallic nanoparticles.

1. Introduction

Nowadays, various industrial processes need fluids with improved heat transfer properties, which have become the key focus of research. Earlier, used fluids like water, oil, and ethylene glycol were among the previously utilized fluids that are not thought to be technologically worthwhile substitutes due to their low heat transfer rates. To enhance the heat transfer rates, nanofluids were made by dispersing a particular kind of nanoparticles-metallic or non-metallic, into them. The term "nanofluid" was first used in 1995 (Choi, 1995). The enhancement of heat transport in a rectangular enclosure using nanofluids has been investigated (Khanafer et al., 2003; Oztop & Abu-Nada, 2008). Additionally, researchers have discovered that by adding several nanoparticles to the base fluid and subsequently creating new, superior working fluids referred to as "hybrid nanofluids," the thermal properties of the nanofluid might be enhanced. Many researchers have

carried out experimental investigations that took into account the hybrid nano-composite particles (Turcu et al., 2006; Jana et al., 2007). A hybrid nanofluid is a sophisticated fluid that combines several nanoparticles, which can increase the rate of heat transmission due to their synergistic effects (Sarkar et al., 2015). The boundary layer flow problem has also been studied in hybrid nanofluid research; for instance, the advantages of using a hybrid nanofluid over a stretching surface have been demonstrated (Devi & Devi, 2016). They discovered that the hybrid nanoparticles increased the rate of heat transmission, and their findings were supported by experimental data (Suresh et al., 2011). Furthermore, a comprehensive review summarizing the role of hybrid nanofluids in heat-transfer enhancement has been presented (Muneeshwaran et al., 2021). Beyond these studies, investigations have examined the thermal instability and convective behaviour of hybrid nanofluids in various configurations. For example, a horizontal composite nanofluid layer was analyzed to determine the critical Rayleigh number for instability (Kumar & Awasthi, 2020). The effects of MHD convection along with internal heat generation/absorption in an inclined porous cavity filled with Al_2O_3–Cu/water nanofluid were studied (Chamkha et al., 2022). These studies demonstrated that, compared to low concentrations, higher volume fractions generally reduce thermal performance. Additionally, the natural convection of a hybrid nanofluid from a sinusoidal wavy cylinder in a curved cavity under a magnetic field was investigated (Parvin et al., 2021), showing that increasing the nanofluid concentration and the Rayleigh number significantly enhance heat transfer, whereas higher Hartmann numbers reduce thermal performance.

Nanofluid convection has been extensively investigated under the local thermal equilibrium (LTE) model. For instance, the convective instability of a horizontal nanofluid layer was analyzed (Nield & Kuznetsov, 2010a). Numerous studies have examined various convective fluid flow problems in nanofluids under the LTE model to assess their stabilizing effects impact (Bhadauria & Agarwal, 2011; Chand & Rana, 2012; Chand & Rana, 2015; Gupta et al., 2015; Ahuja et al., 2016; Sharma et al., 2016; Sharma et al., 2017; Sharma, 2024). However, in many real-world applications, the local thermal non-equilibrium (LTNE) phenomena become significant, such as in textile transport (Ye et al., 2010) and stellar atmospheres (Straughan, 2010). A thermal lag between the nanoparticles and the fluid has been proposed as a governing mechanism of LTNE behaviour (Vadasz, 2006). The LTNE model has been applied to study nanofluid flow through porous enclosures, revealing that temperature gradients and permeability are inversely related (Sheikholeslami & Shehzad, 2018). Similarly, unsteady convection in a partially porous cavity has been analyzed using the LTNE model (Astanina et al., 2019). The impact of LTNE on the convective instability of horizontal nanofluid layers has been demonstrated (Nield & Kuznetsov, 2010b; Sharma & Gupta, 2020), highlighting its destabilizing effect under Hall currents. Further studies have considered the combined effects of rotation and magnetic fields on nanofluid instability under LTNE conditions (Ahuja & Gupta, 2019), and comprehensive reviews have summarized various nanofluid instability problems (Ahuja & Sharma, 2020). The influence of pressure differences on Darcy–Bénard convection under non-equilibrium conditions has also been investigated (Postelnicu, 2010), while the effect of horizontal pressure gradients on convective instability and heat transport in a nano-liquid saturated high-porosity medium has been reported (Sakshath & Joshi, 2021). Finally, gravity modulation effects on Jeffrey and micropolar nanofluids in porous media under LTNE conditions were examined (Shilpee & Bhadauria, 2023, 2024), showing that low modulation frequencies produce shorter intervals that slow convection, whereas higher frequencies result in behaviour comparable to unmodulated conditions."

In many theoretical and experimental studies, understanding the thermal interaction between the solid nanoparticles and the base fluid is crucial for accurately predicting heat-transfer behaviour. In the LTE (Local Thermal Equilibrium) model, the solid and fluid phases are assumed to have identical temperatures at every point, resulting in a single energy equation. In contrast, the LTNE (Local Thermal Non-Equilibrium) model accounts for separate temperatures for the fluid and solid phases, requiring two coupled

energy equations connected through an interphase heat-transfer coefficient. This distinction becomes significant when dealing with nanofluids or porous/hybrid systems where the thermal response of nanoparticles differs from that of the base fluid. Only a limited number of investigations incorporate LTNE effects, and none, to the best of our knowledge, simultaneously consider the influence of LTNE mechanisms and an externally imposed horizontal pressure gradient on hybrid nanofluid convection. The present study addresses this gap by formulating and analyzing a comprehensive LTNE-based model for a horizontal layer saturated with a hybrid nanofluid. Such a configuration has not been explored previously and is scientifically important, as hybrid nanofluid instability under this combined setting introduces richer physics involving interphase heat exchange, multiple nanoparticle species, and pressure-driven transport. Analytical and numerical investigations for various physical properties of the system using metallic and non-metallic nanoparticles in water and ethylene glycol (EG) reveal many interesting and significant results. Various non-dimensional numbers are introduced due to LTNE and the hybrid nature of the system, which is observed to be more affected by the properties of the base fluid as compared to that of particles. Base fluid conductivity enters the process through both LTNE and nanofluid parameters and altogether makes the system highly sensitive, while a denser base fluid makes the system stable. Viscosity affects the process majorly through the Lewis number and destabilizes the system appreciably. These outcomes establish a more comprehensive understanding of convection in hybrid nanofluids under non-equilibrium thermal conditions and highlight the scientific contribution of the present work relative to existing LTE-based studies.

2. Mathematical Formulation

In this study, an infinite horizontal layer of hybrid nanofluid (consisting of a base fluid suspended with two different nanoparticles) is considered. The layer is confined between $z = 0$ and $z = d$, heated from below and cooled from above. The temperature at the bottom layer of the nanofluid is maintained at T_h and at the upper layer is T_c $(T_h > T_c)$. The model under consideration is revised to include LTNE effects, which means that the temperature gradient at any location between the phases is significant. Thus, the conservation equations governing the system are (Buongiorno, 2006; Nield & Kuznetsov, 2010b; Chandrasekhar, 1981):

$$\nabla . q = 0 \tag{1}$$

$$\rho_{fo}\left[\frac{\partial q}{\partial t} + (q.\nabla)q\right] = -\nabla p + \mu \nabla^2 q + \rho_{nl} g \tag{2}$$

$$\begin{aligned}(\rho c)_f\left[\frac{\partial T_f}{\partial t} + q.\nabla T_f\right] = k_f \nabla^2 T_f + (\rho c)_{p1}\left[D_{B1}\nabla\phi_1.\nabla T_f + \frac{D_{T1}}{T_f}\nabla T_f.\nabla T_f\right] + \\ (\rho c)_{p2}\left[D_{B2}\nabla\phi_2.\nabla T_f + \frac{D_{T2}}{T_f}\nabla T_f.\nabla T_f\right] + \frac{h_{fp1}}{1-\phi_0}(T_{p1} - T_f) + \frac{h_{fp2}}{1-\phi_0}(T_{p2} - T_f)\end{aligned} \tag{3}$$

$$\phi_0 (\rho c)_{p1}\left[\frac{\partial T_{p1}}{\partial t} + q.\nabla T_{p1}\right] = \phi_0 k_{p1}\nabla^2 T_{p1} + h_{fp_1}(T_f - T_{p1}) \tag{4}$$

$$\phi_0 (\rho c)_{p2}\left[\frac{\partial T_{p2}}{\partial t} + q.\nabla T_{p2}\right] = \phi_0 k_{p2}\nabla^2 T_{p2} + h_{fp2}(T_f - T_{p2}) \tag{5}$$

$$\frac{\partial \phi_1}{\partial t} + (q.\nabla)\phi_1 = D_{B1}\nabla^2\phi_1 + \frac{D_{T1}}{T_c}\nabla^2 T_f \tag{6}$$

$$\frac{\partial \phi_2}{\partial t}+\left(q.\nabla\right)\phi_2 = D_{B2}\nabla^2\phi_2+\frac{D_{T2}}{T_c}\nabla^2 T_f \tag{7}$$

$$\text{where, } \rho_{nl}=\phi_1\rho_{p1}+\phi_2\rho_{p2}+(1-\phi_1-\phi_2)\rho_f;\ \rho_f=\left[1-\beta(T_{nl}-T_c)\right]\rho_{fo},\ \text{and}\ g=(0,0,-g) \tag{8}$$

Here $q, g, t, p, \mu, \rho_{nl}, \rho_f$ represent the nanofluid velocity, acceleration due to gravity, time, pressure, viscosity, and density of base fluid and nanofluid, ϕ_1, ϕ_2 represent the volume fraction of nanoparticles at the lower and upper boundaries, T_{p1}, T_{p2} are the temperatures of the particles respectively. Further, D_{B1}, D_{B2} represents the Brownian diffusion coefficients, D_{T1}, D_{T2} are the thermophoretic diffusion coefficients, ρ_{p1}, ρ_{p2} are the nano-particles mass density, k_f, k_{p1}, k_{p2} are the thermal conductivities of the fluid and particle phases, h_{fp1}, h_{fp2} are the interphase heat transfer coefficient between the fluid and particle phases. Also, we assumed that the nano-particle volume fractions do not vary on both boundaries and a pressure gradient is applied in the horizontal direction. Therefore, the conditions for both free boundaries are

$$w=0, \frac{\partial w}{\partial z}+\lambda_1 d\frac{\partial^2 w}{\partial z^2}=0, T=T_o+\Delta T, \phi_1=\phi_{10}, \phi_2=\phi_{20}\ at\ z=0 \tag{9}$$

$$w=0, \frac{\partial w}{\partial z}-\lambda_2 d\frac{\partial^2 w}{\partial z^2}=0, T=T_o, \phi_1=\phi_{11}, \phi_2=\phi_{21}\ at\ z=d \tag{10}$$

Now the Equations (1)-(8) are non-dimensionalized using

$$\left(x^*, y^*, z^*\right)=\frac{(x,y,z)}{d}, t^*=\frac{t\alpha_f}{d^2}, \left(u^*, v^*, w^*\right)=\frac{(u,v,w)}{\alpha_f}d, p^*=\frac{pd^2}{\mu\alpha_f}, T^*=\frac{T-T_c}{T_h-T_c}, T_f{}^*=\frac{T_f-T_c}{T_h-T_c}, T_{p1}{}^*=\frac{T_{p1}-T_c}{T_h-T_c},$$

$$T_{p2}{}^*=\frac{T_{p2}-T_c}{T_h-T_c}, \phi_1^*=\frac{\phi_1-\phi_{10}}{\phi_{11}-\phi_{10}}, \phi_2^*=\frac{\phi_2-\phi_{20}}{\phi_{21}-\phi_{20}} \tag{11}$$

Using Equation (11) in Equations (1)-(8) we get (dropping '*')

$$\nabla.q=0 \tag{12}$$

$$\frac{1}{\mathrm{Pr}}\left[\frac{\partial}{\partial t}\left(\nabla^2\psi\right)\right]=\nabla^4\psi-Rn_1\frac{\partial \phi_1}{\partial x}-Rn_2\frac{\partial \phi_2}{\partial x}+Ra\frac{\partial T}{\partial x} \tag{13}$$

$$\begin{aligned}\frac{\partial T_f}{\partial t}-\frac{\partial \psi}{\partial z}\frac{\partial T_f}{\partial x}+\frac{\partial \psi}{\partial x}\frac{\partial T_f}{\partial z}=\nabla^2 T_f+\frac{Nb_1}{Le_1}\nabla\phi_1.\nabla T_f+\frac{Na_1Nb_1}{Le_1}\nabla T_f.\nabla T_f+\frac{Nb_2}{Le_2}\nabla\phi_2.\nabla T_f+\\ \frac{Na_2Nb_2}{Le_2}\nabla T_f.\nabla T_f+N_1\left(T_{p1}-T_f\right)+N_2\left(T_{p2}-T_f\right)\end{aligned} \tag{14}$$

$$\frac{\partial T_{p1}}{\partial t}-\frac{\partial \psi}{\partial z}\frac{\partial T_{p1}}{\partial x}+\frac{\partial \psi}{\partial x}\frac{\partial T_{p1}}{\partial z}=e_1\nabla^2 T_{p1}+N_1 r_1\left(T_f-T_{p1}\right) \tag{15}$$

$$\frac{\partial T_{p2}}{\partial t}-\frac{\partial \psi}{\partial z}\frac{\partial T_{p2}}{\partial x}+\frac{\partial \psi}{\partial x}\frac{\partial T_{p2}}{\partial z}=e_2\nabla^2 T_{p2}+N_2 r_2\left(T_f-T_{p2}\right) \tag{16}$$

$$\frac{\partial \phi_1}{\partial t}-\frac{\partial \psi}{\partial z}\frac{\partial \phi_1}{\partial x}+\frac{\partial \psi}{\partial x}\frac{\partial \phi_1}{\partial z}=\frac{1}{Le_1}\nabla^2\phi_1+\frac{Na_1}{Le_1}\nabla^2 T \tag{17}$$

$$\frac{\partial \phi_2}{\partial t}-\frac{\partial \psi}{\partial z}\frac{\partial \phi_2}{\partial x}+\frac{\partial \psi}{\partial x}\frac{\partial \phi_2}{\partial z}=\frac{1}{Le_2}\nabla^2\phi_2+\frac{Na_2}{Le_2}\nabla^2 T \tag{18}$$

where, ψ is the non-dimensional stream function defined to satisfy the continuity equation, is given by

$u=-\frac{\partial \psi}{\partial z}, w=\frac{\partial \psi}{\partial x}$, and

$$Rm=(\phi_{10}\rho_{p_1}+\phi_{20}\rho_{p_2}+(1-\phi_{10}-\phi_{20})\rho_{f_0})\frac{gd^3}{\mu\alpha_f},\ Rn_1=(\phi_{11}-\phi_{10})(\rho_{p_1}-\rho_{f_0})\frac{gd^3}{\mu\alpha_f},\ \Pr=\frac{\mu}{\rho_{f0}\alpha_f},$$

$$Rn_2=(\phi_{21}-\phi_{20})(\rho_{p_2}-\rho_{f_0})\frac{gd^3}{\mu\alpha_f},\ Ra=(T_h-T_c)(1-\phi_{10}-\phi_{20})\frac{gd^3}{\mu\alpha_f},\ Le_1=\frac{\alpha_f}{D_{B_1}},\ Le_2=\frac{\alpha_f}{D_{B_2}},$$

$$Nb_1=\frac{(\rho c)_{p_1}(\phi_{11}-\phi_{10})}{(\rho c)_f}, Nb_2=\frac{(\rho c)_{p_2}(\phi_{21}-\phi_{20})}{(\rho c)_f}, Na_1=\frac{D_{T_1}(T_h-T_c)}{T_c D_{B_1}(\phi_{11}-\phi_{10})},\ Na_2=\frac{D_{T_2}(T_h-T_{c)}}{T_c D_{B_2}(\phi_{21}-\phi_{20})},$$

$$r_1=\frac{(1-\phi_0)(\rho c)_f}{\phi_0(\rho c)_{p_1}}, r_2=\frac{(1-\phi_0)(\rho c)_f}{\phi_0(\rho c)_{p_2}},\ e_1=\frac{k_{p1}(\rho c)_f}{k_f(\rho c)_{p1}}, e_2=\frac{k_{p2}(\rho c)_f}{k_f(\rho c)_{p2}},$$

$$N_1=\frac{h_{f_{p1}}d^2}{(1-\phi_0)K_f}, N_2=\frac{h_{f_{p2}}d^2}{(1-\phi_0)K_f} \tag{19}$$

The symbol Rm denotes the basic density Rayleigh number, Pr is the Prandtl number, Ra is the thermal Rayleigh number. The nanofluid parameters: Rn_1, Rn_2 are the concentration Rayleigh numbers representing buoyancy effects due to nanoparticle concentration gradients, Le_1, Le_2 are the Lewis numbers defined as the ratio of thermal diffusivity to Brownian diffusion coefficient, Nb_1, Nb_2 are the modified particle-density increments accounting for density variations introduced by nanoparticles, Na_1, Na_2 are the modified diffusivity ratios describing the relative diffusivities of the nanoparticle species in the base fluid. The LTNE parameters: r_1, r_2 are the modified thermal capacity ratios describing the relative heat capacities of the fluid phase and particle phase, e_1, e_2 are the thermal diffusivity ratios of the thermal diffusivity of the nanoparticle phase to that of the fluid phase, N_1, N_2 are the interphase heat transfer parameters or Nield numbers which quantify the rate of heat exchange between the solid (or nanoparticle) phase and the fluid phase in the two-temperature model. The boundary conditions become

$$\psi=D^2\psi=0, T_f=T_{p1}=T_{p2}=1, \phi_1=\phi_2=0, \text{ at } z=0 \tag{20}$$

$$\psi=D^2\psi=T_f=T_{p1}=T_{p2}=0, \phi_1=\phi_2=1, \text{at } z=1 \tag{21}$$

3. Basic State and Perturbation Equations

Initially, the physical quantities vary in the vertical direction only and the magnitude of horizontal pressure gradient to be Π . Also, for the basic state, no heat transfer takes place i.e. $N_1 = N_2 = 0$ Thus, the basic state is described by

$$q_b = (\Pi, 0, 0), p = p_b(z), T_f = T_{fb}(z), T_{p1} = T_{pb1}(z), T_{p2} = T_{pb2}(z), \phi_1 = \phi_{1b}(z), \phi_2 = \phi_{2b}(z) \tag{22}$$

Using Equation (22) in Equations (13)-(18), we get

$$T_{pb1} = T_{pb2} = T_{fb} = 1 - z, \phi_{1b} = \phi_{2b} = z, \psi_b = -\Pi\left(z - \frac{1}{2}\right) \tag{23}$$

where, the chosen integration constant for the stream function ψ is such that, ψ is anti-symmetric about $z = 1/2$. Now let us write

$$q = q_b + q' = (\Pi + u', v', w'), \phi_1 = \phi_{1b} + \phi_1', \phi_2 = \phi_{2b} + \phi_2', T_f = T_{fb} + T_f'$$
$$T_{p1} = T_{pb1} + T_{p1}', T_{p2} = T_{pb2} + T_{p2}', \psi = \psi_b + \psi' \tag{24}$$

Applying perturbations as described in Equation (24) to the set of Equations (12)-(18) and using basic state solution given in Equation (23), we get new set of perturbed equations as

$$\frac{1}{\Pr}\left(\frac{\partial}{\partial t}\nabla^2\psi'\right) = \nabla^4\psi' - Rn_1\frac{\partial \phi_1'}{\partial x} - Rn_2\frac{\partial \phi_2'}{\partial x} + Ra\frac{\partial T'}{\partial x} \tag{25}$$

$$\frac{\partial T_f'}{\partial t} + \Pi\frac{\partial T_f'}{\partial x} - \frac{\partial \psi'}{\partial x} = \nabla^2 T_f' + \frac{Nb_1}{Le_1}\left(\frac{\partial T_f'}{\partial z} - \frac{\partial \phi_1'}{\partial z}\right) - 2\frac{Na_1 Nb_1}{Le_1}\left(\frac{\partial T_f'}{\partial z}\right) + \frac{Nb_2}{Le_2}\left(\frac{\partial T_f'}{\partial z} - \frac{\partial \phi_2'}{\partial z}\right) - 2\frac{Na_2 Nb_2}{Le_2}\left(\frac{\partial T_f'}{\partial z}\right) + N_1\left(T_{P_1}' - T_f'\right) + N_2\left(T_{p2}' - T_f'\right) \tag{26}$$

$$\frac{\partial T_{p1}'}{\partial t} + \Pi\frac{\partial T_{p1}'}{\partial x} - \frac{\partial \psi'}{\partial x} = e_1\nabla^2 T_{p1}' + N_1 r_1\left(T_f' - T_{p1}'\right) \tag{27}$$

$$\frac{\partial T_{p2}'}{\partial t} + \Pi\frac{\partial T_{p2}'}{\partial x} - \frac{\partial \psi'}{\partial x} = e_2\nabla^2 T_{p2}' + N_2 r_2\left(T_f' - T_{p2}'\right) \tag{28}$$

$$\frac{\partial \phi_1'}{\partial t} + \Pi\frac{\partial \phi_1'}{\partial x} + \frac{\partial \psi'}{\partial x} = \frac{1}{Le_1}\nabla^2\phi_1 + \frac{Na_1}{Le_1}\nabla^2 T_f' \tag{29}$$

$$\frac{\partial \phi_2'}{\partial t} + \Pi\frac{\partial \phi_2'}{\partial x} + \frac{\partial \psi'}{\partial x} = \frac{1}{Le_2}\nabla^2\phi_2' + \frac{Na_2}{Le_2}\nabla^2 T_f' \tag{30}$$

Equations (25)-(30) are solved using normal mode technique in the subsequent section.

4. Linear Stability Analysis

Let the variables be

$$\left(\psi', T_f', T_{p1}', T_{p2}', \phi_1', \phi_2'\right) = \left[\Psi(z), \Theta_f(z), \Theta_{p1}(z), \Theta_{p2}(z), \Phi_1(z), \Phi_2(z)\right] e^{iv(x-\Pi t)} \tag{31}$$

Substituting Equation (31) in Equations (25)-(30), we get

$$\frac{1}{\mathrm{Pr}}(-iv\Pi)\left(D^2 - v^2\right)\Psi(z) = \left(D^2 + v^2\right)^2 \Psi(z) - Rn_1 iv\Phi_1(z) - Rn_2 iv\Phi_2(z) + Raiv\Theta_f(z) \tag{32}$$

$$-iv\Psi(z) = e_1\left(D^2 - v^2\right)\Theta_{p1}(z) + N_1 r_1\left(\Theta_f(z) - \Theta_{p1}(z)\right) \tag{33}$$

$$-iv\Psi(z) = e_2\left(D^2 - v^2\right)\Theta_{p2}(z) + N_2 r_2\left(\Theta_f(z) - \Theta_{p1}(z)\right) \tag{34}$$

$$iv\Psi(z) = \frac{1}{Le_1}\left(D^2 - v^2\right)\Phi_1(z) + \frac{Na_1}{Le_1}\left(D^2 - v^2\right)\Theta_f(z) \tag{35}$$

$$iv\Psi(z) = \frac{1}{Le_2}\left(D^2 - v^2\right)\Phi_2(z) + \frac{Na_2}{Le_2}\left(D^2 - v^2\right)\Theta_f(z) \tag{36}$$

The one-term Galerkin method is used to solve Equations (32)-(36). Let the trial functions be (satisfying Equations (20) and (21))

$$\Psi = A_1 \sin \pi z, \Phi_1 = A_2 \sin \pi z, \Phi_2 = A_3 \sin \pi z, \Theta_f = A_4 \sin \pi z, \Theta_{p1} = A_5 \sin \pi z, \Theta_{p2} = A_6 \sin \pi z \tag{37}$$

Putting Equation (37) in Equations (32)-(36), and following the process of orthogonalisation, we get

$$\left(\frac{iv\Pi}{\mathrm{Pr}}\left(\pi^2 + v^2\right) - \left(\pi^2 + v^2\right)^2\right) A_1 + ivRn_1 A_2 + ivRn_2 A_3 - ivRa\, A_4 = 0 \tag{38}$$

$$ivA_1 + \frac{1}{Le_1}\left(\pi^2 + v^2\right) A_2 + \frac{Na_1}{Le_1}\left(\pi^2 + v^2\right) A_4 = 0 \tag{39}$$

$$ivA_1 + \frac{1}{Le_1}\left(\pi^2 + v^2\right) A_3 + \frac{Na_2}{Le_2}\left(\pi^2 + v^2\right) A_4 = 0 \tag{40}$$

$$ivA_1 - \left(\pi^2 + v^2\right) A_4 + N_1\left(A_5 - A_4\right) + N_2\left(A_6 - A_4\right) = 0 \tag{41}$$

$$-ivA_1 + \left(e_1\left(\pi^2 + v^2\right) + N_1 r_1\right) A_5 - N_1 r_1 A_4 = 0 \tag{42}$$

$$-ivA_1 + \left(e_1\left(\pi^2 + v^2\right) + N_2 r_2\right) A_6 - N_2 r_2 A_4 = 0 \tag{43}$$

The homogeneous system of Equations (38)-(43) has a non-trivial solution if

$$\begin{vmatrix} \frac{iv\Pi\left(\pi^2+v^2\right)}{\Pr}-\left(\pi^2+v^2\right)^2 & Rn_1iv & Rn_2iv & -Raiv & 0 & 0 \\ iv & \frac{\left(\pi^2+v^2\right)}{Le_1} & 0 & \frac{Na_1\left(\pi^2+v^2\right)}{Le_1} & 0 & 0 \\ iv & 0 & \frac{\left(\pi^2+v^2\right)}{Le_2} & \frac{Na_2\left(\pi^2+v^2\right)}{Le_2} & 0 & 0 \\ -iv & 0 & 0 & \left(\pi^2+v^2\right)+N_1+N_2 & N_1 & N_2 \\ -iv & 0 & 0 & -N_1r_1 & e_1\left(\pi^2+v^2\right)+N_1r_1 & 0 \\ -iv & 0 & 0 & -N_2r_2 & 0 & e_2\left(\pi^2+v^2\right)+N_2r_2 \end{vmatrix}=0 \quad (44)$$

Equation (44) represents the determinant form of the eigenvalue problem. Solving this equation and retaining only the real part associated with the stationary mode (i.e., the non-oscillatory branch where the growth rate is real) yields the expression for the Rayleigh number as:

$$Ra=\frac{J^3}{v^2}\frac{a_1}{a_2}-\frac{Rn_1(Le_1a_1+Na_1a_2)+Rn_2(Le_2a_1+Na_2a_2)}{a_2} \quad (45)$$

where, $J=\pi^2+v^2$.

$$a_1=e_1e_2J^2+e_1e_2J\left(N_1+N_2\right)+e_2N_1r_1\left(J+N_2\right)+e_1N_2r_2\left(J+N_1\right)+N_1N_2r_1r_2 \quad (46)$$

$$a_2=e_1e_2J^2+e_2JN_1\left(1+r_1\right)+e_1JN_2\left(1+r_2\right)+N_1N_2r_2+N_1N_2r_1\left(1+r_2\right) \quad (47)$$

Further, the obtained expression of the Rayleigh number for the hybrid nanofluid system given by Equations (45), (46) and (47) are validated using previous studies available in the literature. On substituting nanofluid parameters $Rn_2=0, N_2=0$, the expression reduces to the Rayleigh number for mono nanofluid under LTNE effects

$$Ra=\frac{J^3}{v^2}\frac{\left(e_1J+N_1\left(e_1+r_1\right)\right)}{\left(e_1J+N_1\left(1+r_1\right)\right)}-Rn_1\left(\frac{Le_1\left(e_1J+N_1\left(e_1+r_1\right)\right)}{\left(e_1J+N_1\left(1+r_1\right)\right)}+Na_1\right) \quad (48)$$

which is the same as obtained by Nield & Kuznetsov (2010) and Sharma & Gupta (2020), in the absence of Hall currents and hence the validity of the present expression is established.

Let us further eliminate the LTNE parameters from Equations (48) by putting $Rn_2=0, N_1=N_2=0$, the Equation (45) for mono nanofluid under LTE effects becomes

$$Ra=\frac{J^3}{v^2}-Rn_1\left(Le_1+Na_1\right) \quad (49)$$

which agrees with Nield and Kuznetsov (2010a) and validates the derived expression of the Rayleigh number (Equation (49)).

Let us substitute LTNE parameters zero (i.e. $N_1=N_2=0$) in Equation (45), the expression of the Rayleigh number for the hybrid nanofluid under the LTE case reduces to

$$Ra=\frac{J^3}{v^2}-Rn_1\left(Le_1+Na_1\right)-Rn_2\left(Le_2+Na_2\right) \quad (50)$$

Thus, on comparing Equations (49) and (50) show that the hybrid character of fluid reduces the value of the Rayleigh number further as compared to mono nanofluids. This establishes that the presence of multiple nanoparticles in the fluid makes the system even less sensitive, thereby enhancing the destabilizing thermal transport mechanisms.

5. Numerical Analysis and Discussion

In this section, Equation (45) is analysed numerically using the software Mathematica and graphs are drawn to explore the impact of various factors which are involved in the convection process of the fluid layer. Here, water and ethylene glycol are selected as base liquids because they are the most widely used heat-transfer fluids in engineering and industrial applications, providing a meaningful basis for comparison. They also possess distinctly different thermophysical properties—particularly viscosity, thermal conductivity, and specific heat—which allow us to clearly examine how base-fluid characteristics influence the stability behaviour of mono and hybrid nanofluids under LTNE conditions. Including both fluids, therefore, enables a broader and more realistic assessment of convection performance across low-viscosity (water) and high-viscosity (ethylene glycol) base media. To support this analysis, **Table 1** summarises the thermophysical properties of the nanoparticles (metallic/non-metallic) and the selected base liquids (water and ethylene glycol) used in the study.

Table 1. Thermophysical properties of nanoparticles and base liquids at 293 K.

Property	Water	Ethylene Glycol	Al_2O_3	TiO_2	Cu	Ag
Specific heat (J/kg K)	4181	2383	765	692	385	235
Density (kg/m3)	997	1115	3970	4175	8933	10500
Thermal conductivity (W/m K)	0.613	0.252	40	8.4	401	429
Viscosity (kg/m s)	0.001	0.0157	-	-	-	-

5.1 Effect of Various Parameters on Alumina-Titanium Dioxide/ Water Hybrid Nanofluid

Let us begin the section with the investigations of effects of various non-dimensional numbers (Equation (19)) on the stability of the hybrid nanofluid with water as base liquid and both the particles as non-metallic; aluminium and titanium dioxide. Numerical values of the physical parameters for the aluminium and titanium dioxide nanoparticles are calculated using **Table 1**, which are $e_1 = 82$, $e_2 = 18$, $N_1 = 15$, $N_2 = 15$, $r_1 = 122$, $r_2 = 128$, $Le_1 = 530$, $Le_2 = 530$, $Na_1 = 0.4$, $Na_2 = 2$, $Rn_1 = 0.018$, $Rn_2 = 0.019$. All graphical results presented in this work are obtained directly from the analytical expressions and numerical computations developed in the present study. **Figure 1** establishes the destabilizing effect of the modified thermal capacity ratio, and the stabilizing impact of the Nield number is observed in **Figure 2**.

The stabilizing effect of thermal diffusivity ratio (**Figure 3**) and destabilizing nature of concentration Rayleigh number (**Figure 4**) are established. Lewis number is shown to have a destabilizing influence (**Figure 5**), while there is a slight destabilizing effect of the modified thermal diffusivity ratio, which is not reflected in **Figure 6**. Thus, all the non-dimensional numbers (Equation (19)) mainly have a destabilizing effect on the layer except for the thermal diffusivity ratio (e) and Nield number (N), which are found to have a strong stabilizing effect. Let us study the convection process further in detail to explore the effect of various physical properties of nanoparticles and base liquids on the sensitivity of the system.

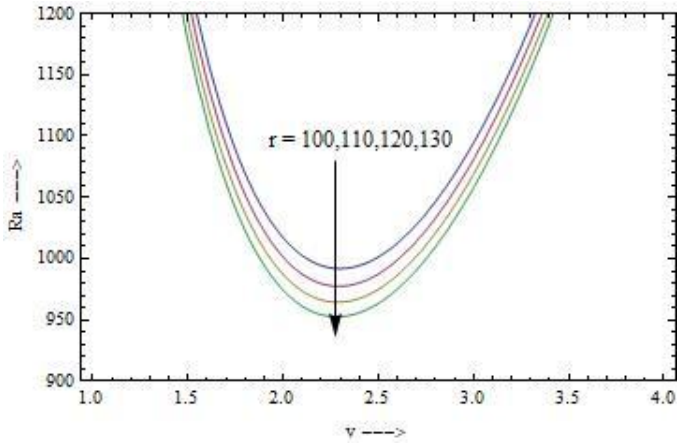

Figure 1. Curves for modified thermal capacity ratio (*r*).

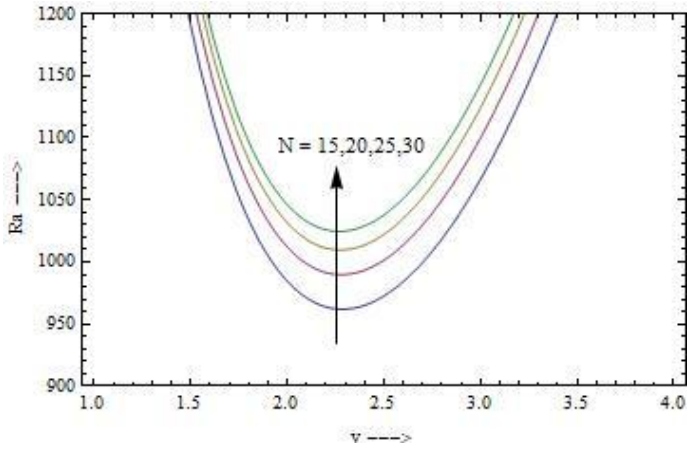

Figure 2. Curves for Nield number (*N*).

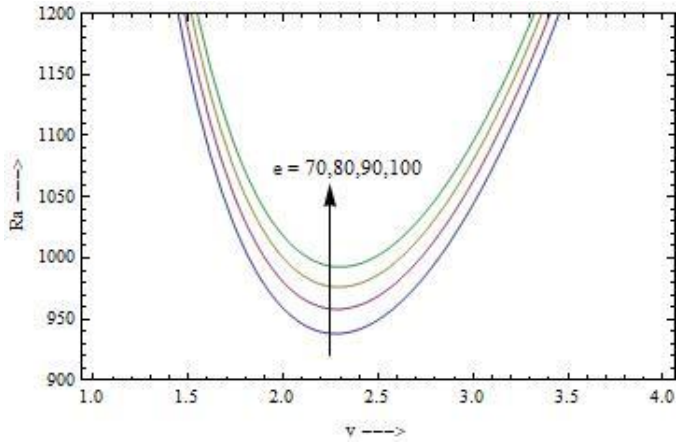

Figure 3. Curves for thermal diffusivity ratio (*e*).

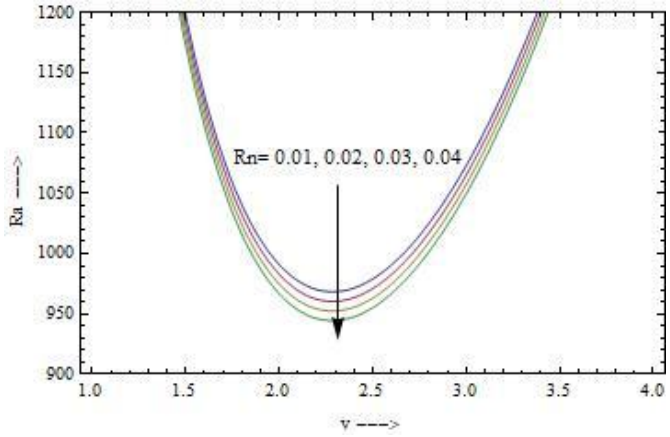

Figure 4. Curves for concentration Rayleigh number (*Rn*).

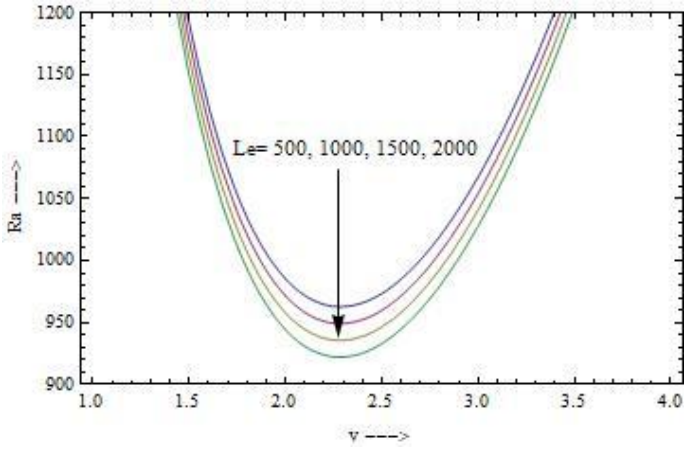

Figure 5. Curves for Lewis number (*Le*).

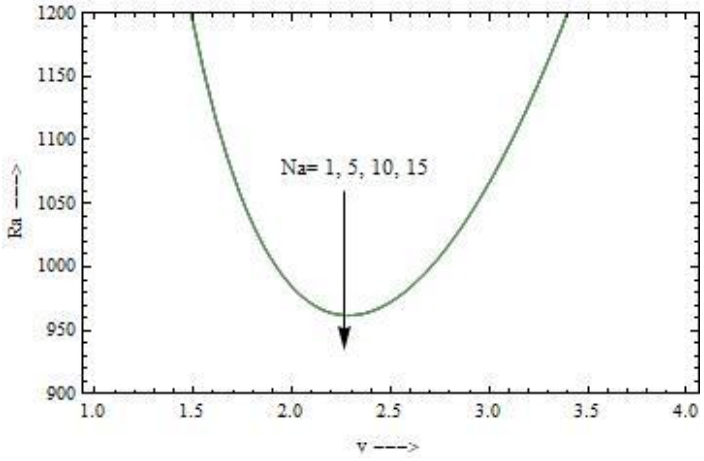

Figure 6. Curves for modified thermal diffusivity ratio (*Na*).

5.2 Effect of Various Physical Properties on Alumina-Titanium Dioxide/ Water Hybrid Nanofluid

The values of various parameters are calculated and presented in **Tables 2-5** for Equation (19)) using thermos-physical properties of alumina-titanium dioxide/water given in **Table 1**. In the subsequent analysis, the symbols '↑' denotes the increase in the values and the symbol '↓' denotes the decrease in the values of corresponding parameters. **Figure 7** is drawn using **Table 2** to show the effect of variation in base fluid conductivity on the Rayleigh number for the system. As k_f↑; the affected non-dimensional numbers e_1↓, e_2↓, N_1↓, N_2↓, Le_1↑, Le_2↑, Na_1↑, Na_2↑ (**Table 2**). **Figure 7** is drawn using **Table 2** to show the effect of variation in base fluid conductivity on the Rayleigh number for the system. As k_f↑; the affected non-dimensional numbers e_1↓, e_2↓, N_1↓, N_2↓, Le_1↑, Le_2↑, Na_1↑, Na_2↑ (**Table 2**). As e↓⇒Ra ↓ (**Figure 3**), N↓⇒Ra ↓ (**Figure 2**), Le↑⇒ Ra ↓ (**Figure 5**), and Na↑⇒ Ra↓ (**Figure 6**). Thus, all the involved parameters *e, N, Le, Na* contributes to decreasing the values of *Ra* and hence stability of the system decreases appreciably with rise in base fluid conductivity. This indicates that enhanced thermal conductivity of the base fluid promotes faster heat diffusion, thereby weakening the buoyancy-driven instability mechanism in the hybrid nanofluid layer.

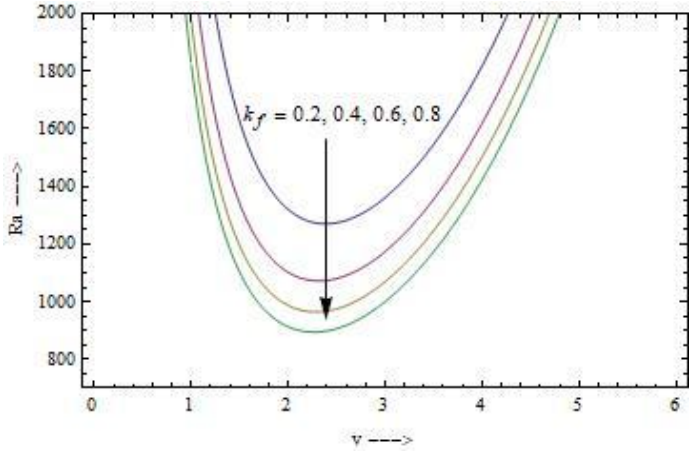

Figure 7. Curves for conductivity of base fluid (k_f).

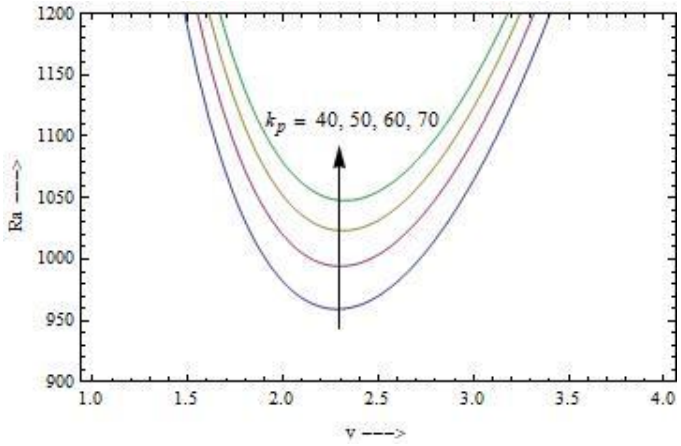

Figure 8. Curves for the conductivity of particles (k_p).

The effect of variation in nanoparticles' conductivity on the Rayleigh number is shown in **Figure 8**. As k_p ↑*;* the affected non-dimensional numbers e_1↑, Na_1↓ (**Table 2**). As e↑⇒Ra ↑ (**Figure 3**), Na↓⇒Ra ↑ (**Figure 6**) and both the parameters postpone the instability phenomenon in the fluid layer, which is consistent with the behaviour of nanoparticles' conductivity as indicated in **Figure 8**.

Table 2. The values of various parameters for variations in the conductivity of base fluid and nanoparticle (Equation (19)).

k_f	e_1	e_2	N_1	N_2	r_1	r_2	Le_1	Le_2	Na_1	Na_2	Rn_1	Rn_2
0.2	274.5	60.5	15.15	15.15	135.8	142.8	159.9	159.9	0.14	0.67	0.017	0.019
0.4	137.2	30.2	7.57	7.57	135.8	142.8	319.8	319.8	0.29	1.28	0.017	0.019
0.6	91.5	20.1	5.05	5.05	135.8	142.8	479.7	479.7	0.43	1.85	0.017	0.019
0.8	68.6	15.14	3.78	3.78	135.8	142.8	639.7	639.7	0.57	2.37	0.017	0.019
k_p	e_1	e_2	N_1	N_2	r_1	r_2	Le_1	Le_2	Na_1	Na_2	Rn_1	Rn_2
40	121.4	20.26	15.15	15.15	180.3	143.26	478.3	478.3	0.43	1.84	0.012	0.019
50	151.8	20.26	15.15	15.15	180.3	143.26	478.3	478.3	0.34	1.84	0.012	0.019
60	182.1	20.2	15.15	15.15	180.3	143.35	478.3	478.3	0.28	1.84	0.012	0.019
70	212.5	20.2	15.15	15.15	180.3	143.2	478.3	478.3	0.24	1.84	0.012	0.019

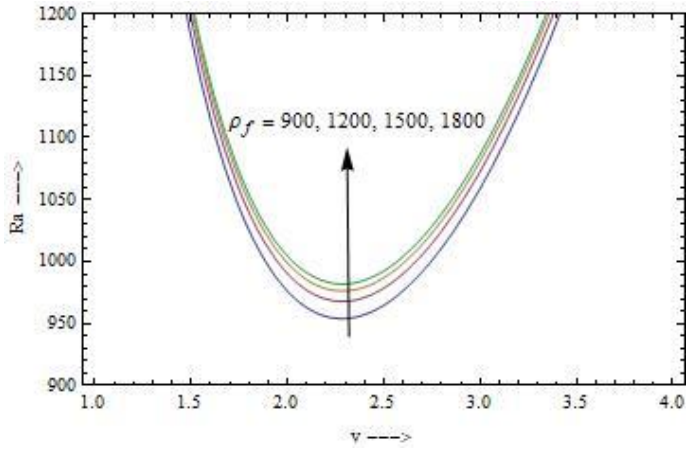

Figure 9. Curves for the density of base fluid (ρ_f).

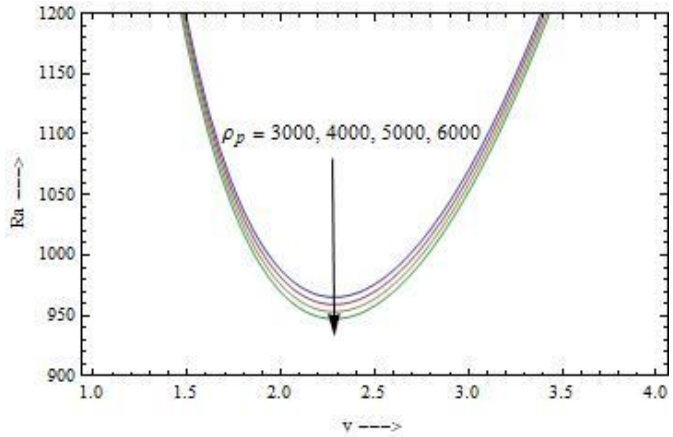

Figure 10. Curves for the density of base fluid (ρ_p).

Table 3. The values of various parameters for variations in the density of base fluid and nanoparticle (Equation (19)).

ρ_f	e_1	e_2	N_1	N_2	r_1	r_2	Le_1	Le_2	Na_1	Na_2	Rn_1	Rn_2
900	82.5	18.2	15.1	15.1	122.6	128.9	531.5	531.5	0.4	2.0	0.018	0.019
1200	110.1	24.3	15.1	15.1	163.5	171.9	398.6	398.6	0.35	1.54	0.016	0.017
1500	137.6	30.3	15.1	15.1	204.4	214.9	318.9	318.9	0.28	1.23	0.014	0.016
1800	165.2	36.4	15.1	15.1	245.3	257.8	265.7	265.7	0.23	1.02	0.013	0.014
ρ_p	e_1	e_2	N_1	N_2	r_1	r_2	Le_1	Le_2	Na_1	Na_2	Rn_1	Rn_2
3000	121.4	20.2	15.15	15.15	180.35	143.26	478.3	478.3	0.430	1.848	0.012	0.019
4000	91.08	20.26	15.15	15.15	135.26	143.26	478.35	478.35	0.430	1.848	0.018	0.019
5000	72.87	20.26	15.15	15.15	108.2	143.26	478.35	478.35	0.430	1.848	0.024	0.019
6000	60.72	20.26	15.15	15.15	90.17	143.26	478.35	478.35	0.430	1.848	0.03	0.019

Figure 9 and **Table 3** show the effect of variation in base fluid density on the thermal Rayleigh number for the system. As $\rho_f\uparrow$; the non-dimensional numbers $e_1\uparrow$, $e_2\uparrow$, $r_1\uparrow$, $r_2\uparrow$, $Le_1\downarrow$, $Le_2\downarrow$, $Na_1\downarrow$, $Na_2\downarrow$, $Rn_1\downarrow$, $Rn_2\downarrow$ (**Table 3**). As $e\uparrow\Rightarrow Ra\uparrow$ (**Figure 3**), $r\uparrow\not\Rightarrow Ra\uparrow$(**Figure 1**), $Le\downarrow\Rightarrow Ra\uparrow$ (**Figure 5**), $Na\downarrow\Rightarrow Ra\uparrow$ (**Figure 6**), $Rn\downarrow\Rightarrow Ra\uparrow$ (**Figure 4**). As a result, the combined effect of all the involved parameters increases the value of '*Ra'* except for the opposing influence of '*r'* and hence stability of the system is enhanced when the base fluid becomes denser.

The influence of particles' density is analysed through **Figure 10** and **Table 3**. As $\rho_p\uparrow$; $e_1\downarrow$, $r_1\downarrow$, $Rn_1\uparrow$ and the trend $e\downarrow\Rightarrow Ra\downarrow$ (**Figure 3**), $r\downarrow\not\Rightarrow Ra\downarrow$ (**Figure 1**), $Rn\uparrow\Rightarrow Ra\downarrow$ (**Figure 4**) is observed. Thus, the density of particles contributes to destabilizing the system (**Figure 10**), which is largely due to the '*e'* and '*Rn'* parameters, which suppress the contradictory impact of parameter '*r*'.

The stability curves for specific heat properties are drawn in **Figures (11)** and **(12)** using the values given in **Table 4** and **Equation (19)**. As $C_f\uparrow$, the parameters $e_1\uparrow$, $e_2\uparrow$, $r_1\uparrow$, $r_2\uparrow$, $Le_1\downarrow$, $Le_2\downarrow$and as $e\uparrow\Rightarrow Ra\uparrow$ (**Figure 3**), $r\uparrow\not\Rightarrow Ra\uparrow$ (**Figure 1**), $Le\downarrow\Rightarrow Ra\uparrow$ (**Figure 5**), Thus, the stabilizing impact of '*e'* and '*Le'* dominates the conflicting effect of '*r'* leading to increase in stability of the system as shown in **Figure 11**. As $C_p\uparrow$, only two numbers $e_1\downarrow$, $r_1\downarrow$and $e\downarrow\Rightarrow Ra\downarrow$ (**Figure 3**), $r\downarrow\not\Rightarrow Ra\downarrow$ (**Figure 1**). The disagreeing effects of *e* and *r* impacts negligibly on the stability of the system, and a slight destabilizing effect of particles' specific heat is established (**Figure 12**).

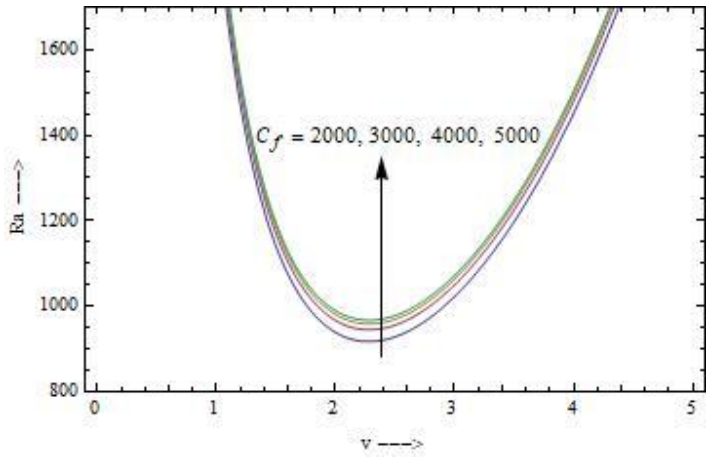

Figure 11. Curves for the specific heat of base fluid (C_f).

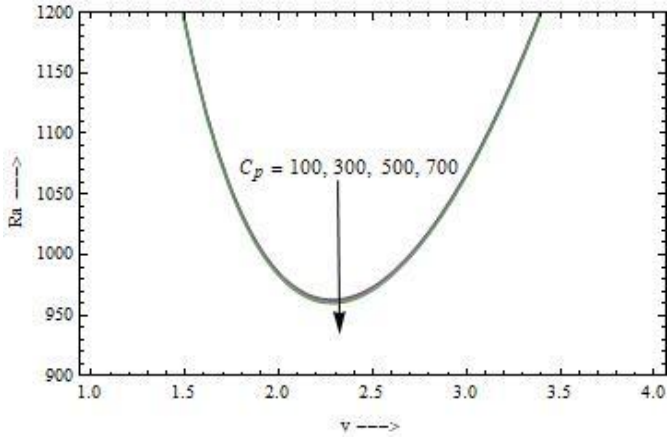

Figure 12. Curves for the specific heat of particles (C_p).

Table 4. The values of various parameters for variations in specific heat of base fluid and nanoparticle (Equation (19)).

C_f	e_1	e_2	N_1	N_2	r_1	r_2	Le_1	Le_2	Na_1	Na_2	Rn_1	Rn_2
2000	43.9	9.69	15.15	15.15	65.19	68.53	1000	1000	0.43	1.848	0.017	0.019
3000	65.8	14.5	15.15	15.15	97.79	102.8	666.66	666.66	0.43	1.848	0.017	0.019
4000	87.8	19.38	15.15	15.15	130.39	137.06	500	500	0.43	1.848	0.017	0.019
5000	109.7	24.22	15.15	15.15	162.98	171.33	400	400	0.43	1.848	0.017	0.019
C_p	e_1	e_2	N_1	N_2	r_1	r_2	Le_1	Le_2	Na_1	Na_2	Rn_1	Rn_2
100	929.11	20.26	15.15	15.15	1379.73	143.26	478.35	478.35	0.430	1.848	0.012	0.019
300	309.7	20.26	15.15	15.15	459.91	143.26	478.35	478.35	0.430	1.848	0.012	0.019
500	185.82	20.26	15.15	15.15	275.9	143.26	478.35	478.35	0.430	1.848	0.012	0.019
700	132.73	20.26	15.15	15.15	197.10	143.26	478.35	478.35	0.430	1.848	0.012	0.019

The impact of base fluid viscosity is analysed through curves drawn in **Figure 13** using the values given in **Table 5**. Viscosity variable enters the system through nano-effects (Brownian diffusion and thermophoresis) and as $\mu_f \uparrow$; $Le_1\uparrow$, $Le_2\uparrow$, $Na_1\uparrow$, $Na_2\uparrow$ (**Table 5**). Also, $Le\uparrow \Rightarrow Ra\downarrow$ (**Figure 5**), $Na\uparrow \Rightarrow Ra\downarrow$ (**Figure 6**). Both the involved parameters decrease the stability, and hence viscous fluids tend to be less stable (**Figure 13**).

Figure 13. Curves for the viscosity of fluid (μ_f).

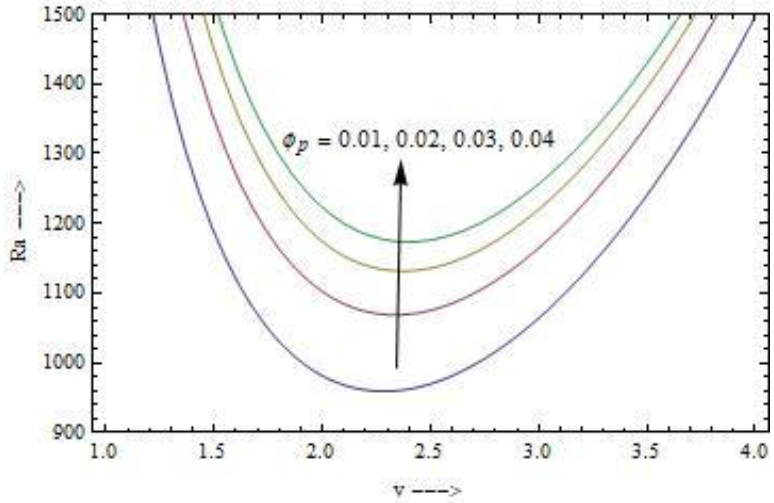

Figure 14. Curves for volume fraction of particles ($\emptyset_p$).

Table 5. The values of various parameters for variations in viscosity and particle volume fraction (Equation (19)).

μ_f	e_1	e_2	N_1	N_2	r_1	r_2	Le_1	Le_2	Na_1	Na_2	Rn_1	Rn_2
0.001	91.77	20.26	15.15	15.15	136.29	143.26	478.35	478.35	0.430	1.848	0.017	0.019
0.002	91.77	20.26	15.15	15.15	136.29	143.26	956.70	956.70	1.723	7.394	0.017	0.019
0.003	91.77	20.26	15.15	15.15	136.29	143.26	1435.06	1435.06	3.876	16.63	0.017	0.019
0.004	91.77	20.26	15.15	15.15	136.29	143.26	1913.42	1913.42	6.892	29.57	0.017	0.019
ϕ_p	e_1	e_2	N_1	N_2	r_1	r_2	Le_1	Le_2	Na_1	Na_2	Rn_1	Rn_2
0.01	91.77	20.26	15.15	15.15	136.29	143.26	478.35	478.35	0.430	1.848	0.017	0.019
0.02	91.77	20.26	15.30	15.15	67.45	143.26	478.35	478.35	0.861	1.848	0.017	0.019
0.03	91.77	20.26	15.46	15.15	44.51	143.26	478.35	478.35	1.292	1.848	0.017	0.019
0.04	91.77	20.26	15.62	15.15	33.04	143.26	478.35	478.35	1.723	1.848	0.017	0.019

Nanoparticles' volume fraction affects the Nield number, modified thermal diffusivity ratio and modified thermal capacity ratio (**Table 5**). As $\phi_p \uparrow$; $N_1 \uparrow$, $r_1 \downarrow$, $Na_1 \uparrow$ and $N \uparrow \Rightarrow Ra \uparrow$ (**Figure 2**), $r \downarrow \Rightarrow Ra \uparrow$ (**Figure 1**), $Na \uparrow \nRightarrow Ra \uparrow$ (**Figure 6**). Out of *N, r* and *Na*, the effect of '*N'* and '*r'* is observed to be dominant over the slightly contradictory impact of '*Na',* and a strong destabilizing influence of particle volume fraction is established (**Figure 14**).

Thus, the above analysis demonstrates that the thermophysical properties of both the particles as well as base fluid play a crucial role in governing the stability of the hybrid nanofluid layer. Small variations in conductivity, density, specific heat, viscosity and particle volume fraction significantly alter key non-dimensional parameters such as LTNE parameters; *e, N, r* and nanofluid parameters; *Le, Na, Rn,* which collectively determine the value of Rayleigh number and hence affect the onset of convection in the layer. Therefore, the study highlights that the small changes in thermophysical properties of the system can appreciably shift the convective instability boundaries, underlining the importance of careful material selection in designing the hybrid nanofluid-based thermal systems.

5.3 Instability Curves for Various Non-Metallic/Metallic Particles + Water/Ethylene Glycol Hybrid Nanofluids

A comparative study of the effects of the LTNE model and LTE model together with hybrid and mono nanofluids is presented in this section. **Figures 15** and **16** are drawn for the stability curves of alumina-titanium dioxide with water and ethylene glycol as base fluids, respectively, using the values of variables calculated in **Table 6**. LTNE effects are found to delay the instability of the system appreciably due to the addition of parameters; modified diffusivity ratio (e), Nield number (N) and modified heat capacity ratio (r) as $e\uparrow\Rightarrow Ra\uparrow$ (**Figure 3**), $N\uparrow\Rightarrow Ra\uparrow$ (Figure 2), $r\uparrow\Rightarrow Ra\uparrow$ (**Figure 1**). Thus, stabilizing effects of 'e' and 'N' suppress the destabilizing influence of 'r', which establishes a more stable system under LTNE effects, as shown in **Figures 15** and **16**. In the case of mono nanofluids, the involved parameters are: $e\uparrow\Rightarrow Ra\uparrow$ (**Figure 3**), $r\uparrow\Rightarrow Ra\downarrow$ (**Figure 1**). and $Rn\uparrow\Rightarrow Ra\downarrow$ (**Figure 4**). Thus, alumina is more stable than titanium dioxide in both the base liquids (**Figures 15** and **16**) because of its higher conductivity and lower density (**Figures 8** and **10**).

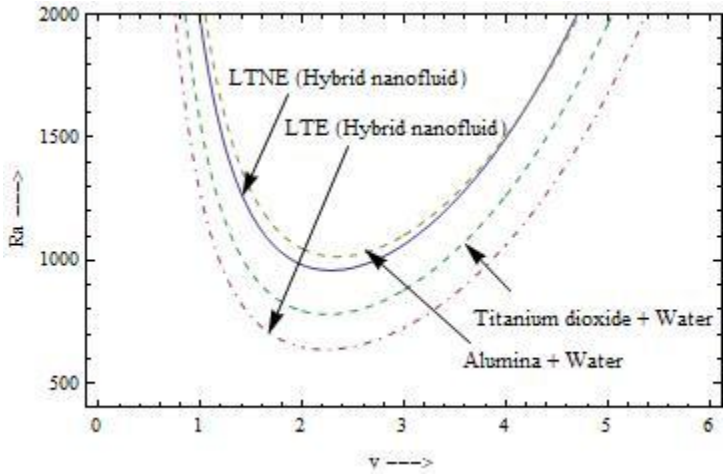

Figure 15. Curves for alumina/titanium dioxide-water.

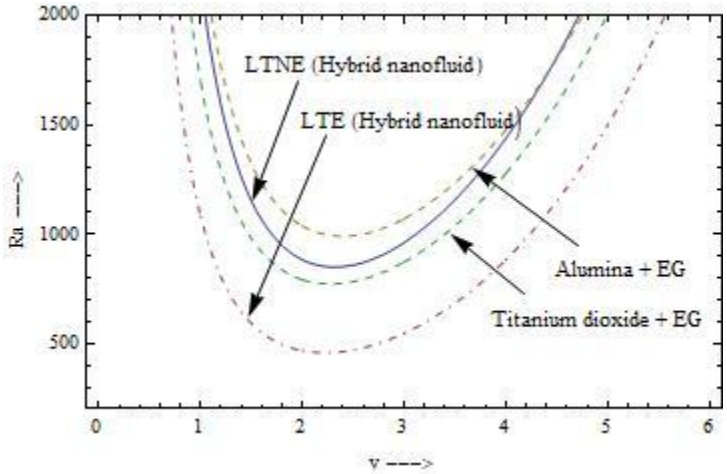

Figure 16. Curves for alumina/titanium dioxide-EG.

Table 6. The values of parameters for Al_2O_3 -TiO_2 with ϕ_0 = 0.01 for hybrid and ϕ_0 = 0.02 for mono fluids (Equation (19)).

Parameters / Fluids	e_1	e_2	N_1	N_2	r_1	r_2	Le_1	Le_2	Na_1	Na_2	Rn_1	Rn_2
Al_2O_3 -TiO_2/Water LTNE (Hybrid)	89.5	19.77	15.15	15.15	135.88	142.83	490.18	490.18	0.44	1.88	0.017	0.019
Al_2O_3 -TiO_2/Water LTE (Hybrid)	0	0	0	0	0	0	490.18	490.18	0.44	1.88	0.017	0.019
Al_2O_3/Water LTNE (Mono)	89.5	0	15.15	0	67.25	0	490.18	0	0.88	0	0.017	0
TiO_2/Water LTNE (Mono)	0	19.77	0	15.30	0	70.69	0	490.18	0	3.76	0	0.019
Al_2O_3 -TiO_2/EG LTNE (Hybrid)	138.86	30.65	12.02	12.02	86.61	91.04	4963.4	4963.4	40.68	185.06	0.017	0.018
Al_2O_3 -TiO_2/EG LTE (Hybrid)	0	0	0	0	0	0	4963.4	4963.4	40.68	185.06	0.017	0.018
Al_2O_3/EG LTNE (Mono)	138.86	0	12.14	0	42.86	0	4963.4	0	81.36	0	0.017	0
TiO_2/EG LTNE (Mono)	0	30.65	0	12.14	0	45.06	0	4963.4	0	370.12	0	0.018

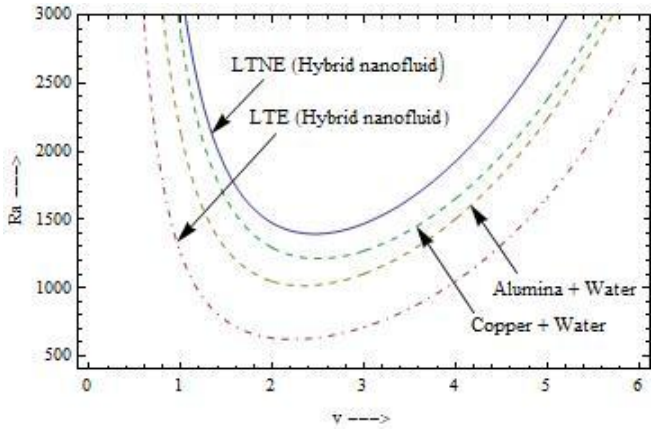

Figure 17. Curves for alumina/copper-water.

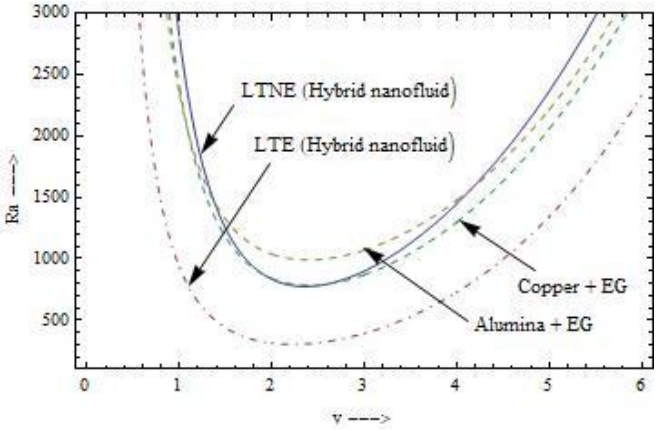

Figure 18. Curves for alumina/copper -EG.

Table 7. The values of parameters for Al_2O_3 -Cu with $\phi_0 = 0.01$ for hybrid and $\phi_0 = 0.02$ for mono fluids (Equation (19)).

Parameters / Fluids	e_1	e_2	N_1	N_2	r_1	r_2	Le_1	Le_2	Na_1	Na_2	Rn_1	Rn_2
Al_2O_3 -Cu/Water LTNE (Hybrid)	89.5	792.86	15.15	15.15	135.8	119.9	490.18	490.18	0.441	0.452	0.017	0.047
Al_2O_3 -Cu/Water LTE (Hybrid)	0	0	0	0	0	0	490.18	490.18	0.441	0.452	0.017	0.047
Al_2O_3/Water LTNE (Mono)	89.5	0	15.15	0	67.25	0	490.18	0	0.88	0	0.017	0
Cu/Water LTNE (Mono)	0	792.86	0	15.30	0	59.39	0	490.18	0	0.90	0	0.047
Al_2O_3 -Cu/EG LTNE (Hybrid)	138.8	1229.3	12.02	12.02	86.61	76.48	4963.4	4963.4	40.68	4.104	0.017	0.046
Al_2O_3 -Cu/EG LTE (Hybrid)	0	0	0	0	0	0	4963.4	4963.4	40.68	4.104	0.017	0.046
Al_2O_3/EG LTNE (Mono)	138.8	0	12.14	0	42.8	0	4963.4	0	81.36	0	0.017	0
Cu/EG LTNE (Mono)	0	1229.3	0	12.14	0	37.85	0	4963.4	0	8.208	0	0.046

Let us consider metallic and non-metallic particles in base liquid (**Figures 17** and **18**) to analyse the effect of composite nanoparticles, i.e. aluminium and copper, in base fluid water (**Figure 17**) and the effect of these nanoparticles in the base fluid ethylene glycol (**Figure 18**). LTNE effects stabilize the alumina/copper-water hybrid nanofluids following the previous case (**Figures 15** and **16**). Copper is observed to be more stable than alumina in water (**Figure 17**) due to the higher conductivity of copper despite having more density whereas the reverse order is observed for ethylene glycol (**Figure 18**) where density acts as the dominant property through concentration Rayleigh number and signifies the contribution of higher values of Lewis number due to more viscosity of ethylene glycol than water.

The effects of both metallic particles are shown in **Figures (19)** and **(20)** using **Table 8**. Copper particles are found to increase the stability in comparison to silver in both **Figures (19)** and **(20)** because of its higher conductivity, which leads to the higher value of '*e*' and stabilizes the layer, while its lesser density destabilizes the system (**Figure 10**).

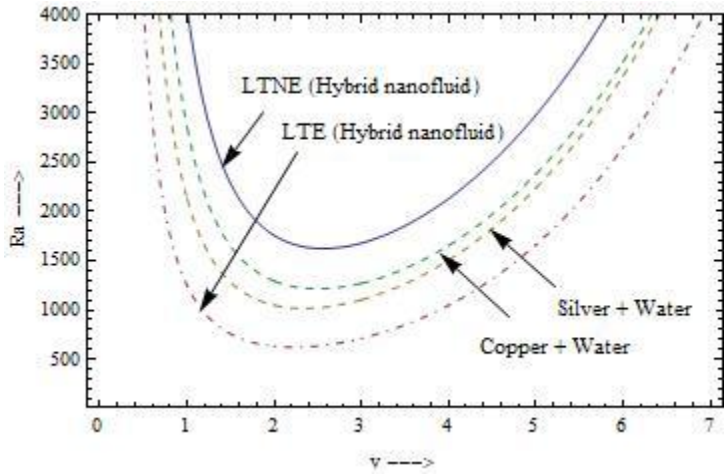

Figure 19. Curves for copper/silver-water.

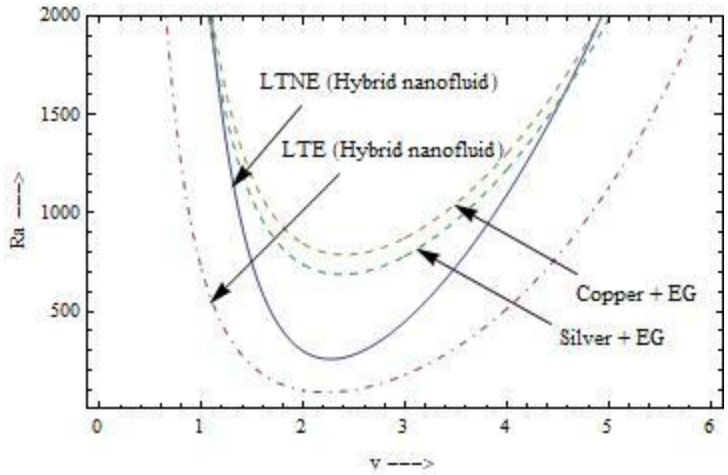

Figure 20. Curves for copper/silver -EG.

It is noteworthy that the hybrid characteristic of fluid makes it less stable as compared to mono nanofluids in the LTE case (Equation (50)), but this is not the case with the LTNE model, as observed in **Figures (15)-(20)**. Also, it is seen in **Figures (15)-(20)** that the curves for ethylene glycol-based fluids are lower than that of water, which establishes water as a more stable fluid than ethylene glycol. Also, note that **Tables 6-8** show *Le* (water) << *Le* (EG), which is affected majorly by the viscosity of the fluid (**Figure 13** and **Table 5**).

Table 8. The values parameters for Cu-Ag with $\phi_0 = 0.01$ for hybrid and $\phi_0 = 0.02$ for mono fluids (Equation (19)).

Parameters / Fluids	e_1	e_2	N_1	N_2	r_1	r_2	Le_1	Le_2	Na_1	Na_2	Rn_1	Rn_2
Cu-Ag/Water LTNE (Hybrid)	792.86	1182.27	15.15	15.15	119.9	167.24	490.18	490.18	0.452	0.042	0.045	0.054
Cu-Ag/Water LTE (Hybrid)	0	0	0	0	0	0	490.18	490.18	0.452	1.889	0.045	0.054
Cu/Water LTNE (Mono)	792.86	0	15.30	0	59.39	0	490.18	0	0.90	0	0.045	0
Ag/Water LTNE (Mono)	0	19.77	0	15.30	0	82.76	0	490.18	0	3.778	0	0.054
Cu-Ag/EG LTNE (Hybrid)	1229.3	1833.15	12.02	12.02	76.48	106.60	4963.4	4963.4	4.104	3.836	0.044	0.053
Cu-Ag/EG LTE (Hybrid)	0	0	0	0	0	0	4963.4	4963.4	4.104	3.836	0.044	0.053
Cu/EG LTNE (Mono)	1229.3	0	12.14	0	37.856	0	4963.4	0	8.208	0	0.044	0
Ag/EG LTNE (Mono)	0	1833.15	0	12.14	0	52.76	0	4963.4	0	7.672		0.053

6. Comparison with Earlier Published Work

The findings of the present study are consistent with earlier investigations on nanofluid convection under both LTE and LTNE frameworks. Previous LTE-based studies have reported that the addition of nanoparticles generally lowers the critical Rayleigh number, thereby promoting earlier onset of convection; our results validate this trend for both mono and hybrid nanofluids. However, LTNE-based works have shown that accounting for separate solid–fluid temperatures leads to a stabilizing influence due to

interphase heat exchange. The present analysis confirms this behaviour, demonstrating that the Nield number and thermal diffusivity ratio significantly delay instability, in agreement with earlier LTNE models. Moreover, studies comparing different base fluids have emphasised the dominant role of viscosity in governing stability, a conclusion that aligns with our comparative assessment of water and ethylene glycol. Similarly, the relative stabilizing or destabilizing effects of alumina, titanium dioxide, copper, and silver nanoparticles observed in our results follow the trends reported in prior literature, particularly regarding the roles of particle conductivity and density. Overall, the present work corroborates established findings while extending them to hybrid nanofluids, thereby offering a broader understanding of convection behaviour under both LTE and LTNE conditions.

7. Conclusions

The present study investigates the onset of convection in hybrid nanofluids under LTE and LTNE conditions using linear stability analysis. The horizontal pressure gradient is shown not influence the stationary mode of instability. LTNE effects, represented primarily through the Nield number and thermal diffusivity ratio, significantly enhance system stability by counteracting the destabilizing influence of nanoparticle-induced parameters such as the concentration, Rayleigh number, Lewis number, and modified thermal diffusivity ratio. While nanoparticles have a tendency to destabilize the layer in the LTE model, the LTNE framework provides a stabilizing mechanism that becomes increasingly dominant. The thermophysical properties of both the base fluid and nanoparticles strongly govern the convection behaviour: higher base-fluid conductivity and viscosity increase sensitivity, whereas larger density and specific heat delay instability. Similarly, greater nanoparticle thermal conductivity and volume fraction strengthen stability, while higher particle density and specific heat weaken it. Water proves to be a more stabilizing base fluid than ethylene glycol due to its lower viscosity, highlighting viscosity as a key controlling factor. Among the nanoparticles, alumina enhances stability more effectively than titanium dioxide, and copper improves the stability of water more than alumina due to its higher conductivity—although this trend reverses for ethylene glycol, where particle density becomes dominant. Silver nanoparticles make the system more sensitive than copper because of their higher density and thermal diffusivity ratio. Overall, the combined effects of LTNE parameters, base-fluid characteristics, and nanoparticle properties reveal the complex interplay governing the stability of mono and hybrid nanofluids.

Conflicts of Interest

The authors declare that they have no known competing financial interests or personal relationships that could have appeared to influence the work reported in this paper.

Acknowledgments

No specific funding was received for conducting this study. The authors also thank the reviewers for their constructive comments and suggestions, which helped improve the quality of the manuscript.

AI Disclosure

The author(s) declare that no assistance is taken from generative AI to write this article.

References

Ahuja, J., & Gupta, U. (2019). Magneto convection in rotating nanofluid layer: local thermal non-equilibrium model. *Journal of Nanofluids*, *8*(2), 430-438.

Ahuja, J., & Sharma, J. (2020). Rayleigh–Bénard instability in nanofluids: a comprehensive review. *Micro and Nano Systems Letters*, *8*(1), 21. https://doi.org/10.1186/s40486-020-00123-y.

Ahuja, J., Sharma, J., Gupta, U., & Wanchoo, R.K. (2016). Hydromagnetic stability of a nanofluid layer using Darcy–Brinkman model. *Journal of Nanofluids, 5*(3), 436-443.

Astanina, M.S., Sheremet, M., & Umavathi, C.J. (2019). Unsteady natural convection in a partially porous cavity having a heat-generating source using local thermal non-equilibrium model. *International Journal of Numerical Methods for Heat & Fluid Flow*, *29*(6), 1902-1919.

Bhadauria, B.S., & Agarwal, S. (2011). Natural convection in a nanofluid saturated rotating porous layer: a nonlinear study. *Transport in Porous Media, 87*(2), 585-602.

Buongiorno, J. (2006). Convective transport in nanofluids. *ASME Journal of Heat Transfer, 128(3)*, 240-250.

Chamkha, A.J., Armaghani, T., Mansour, M.A., Rashad, A., & Kargarsharifabad, H. (2022). MHD convection of an Al_2O_3–Cu/water hybrid nanofluid in an inclined porous cavity with internal heat generation/absorption. *Iranian Journal of Chemistry and Chemical Engineering, 41*(3), 936-956.

Chand, R., & Rana, G.C. (2012). On the onset of thermal convection in rotating nanofluid layer saturating a Darcy–Brinkman porous medium. *International Journal of Heat and Mass Transfer*, *55*(21-22), 5417-5424.

Chand, R., & Rana, G.C. (2015). Magneto convection in a layer of nanofluid in porous medium—a more realistic approach. *Journal of Nanofluids*, *4*(2), 196-202. https://doi.org/10.1166/jon.2015.1142.

Chandrasekhar, S. (1981). *Hydrodynamic and hydromagnetic stability*. Dover Corporation Inc. New York.

Choi, S.U. (1995). Enhancing thermal conductivity of fluids with nanoparticles. In *ASME International Mechanical Engineering Congress and Exposition* (Vol. 17421, pp. 99-105). American Society of Mechanical Engineers. California, USA.

Devi, S.A., & Devi, S.S.U. (2016). Numerical investigation of hydromagnetic hybrid Cu–Al2O3/water nanofluid flow over a permeable stretching sheet with suction. *International Journal of Nonlinear Sciences and Numerical Simulation*, *17*(5), 249-257.

Gupta, U., Sharma, J., & Sharma, V. (2015). Instability of binary nanofluid with magnetic field. *Applied Mathematics and Mechanics, 36*(6), 693-706.

Jana, S., Salehi-Khojin, A., & Zhong, W.H. (2007). Enhancement of fluid thermal conductivity by the addition of single and hybrid nano-additives. *Thermochimica Acta*, *462*(1-2), 45-55.

Khanafer, K., Vafai, K., & Lightstone, M. (2003). Buoyancy-driven heat transfer enhancement in a two-dimensional enclosure utilizing nanofluids. *International Journal of Heat and Mass Transfer*, *46*(19), 3639-3653.

Kumar, V., & Awasthi, M.K. (2020). Thermal instability in a horizontal composite nano-liquid layer. *SN Applied Sciences*, *2*(3), 380. https://doi.org/10.1007/s42452-020-2028-5.

Muneeshwaran, M., Srinivasan, G., Muthukumar, P., & Wang, C.C. (2021). Role of hybrid-nanofluid in heat transfer enhancement–A review. *International Communications in Heat and Mass Transfer*, *125*, 105341. https://doi.org/10.1016/j.icheatmasstransfer.2021.105341.

Nield, D.A., & Kuznetsov, A. (2010a). The onset of convection in a horizontal nanofluid layer of finite depth. *European Journal of Mechanics-B/Fluids*, *29*(3), 217-223.

Nield, D.A., & Kuznetsov, A.V. (2010b). The effect of local thermal nonequilibrium on the onset of convection in a nanofluid. *Journal of Heat Transfer, 132(5)*, 052405. https://doi.org/10.1115/1.4000474.

Oztop, H.F., & Abu-Nada, E. (2008). Numerical study of natural convection in partially heated rectangular enclosures filled with nanofluids. *International Journal of Heat and Fluid Flow*, *29*(5), 1326-1336.

Parvin, S., Roy, N.C., & Saha, L.K. (2021). Magnetohydrodynamic natural convection of a hybrid nanofluid from a sinusoidal wavy cylinder placed in a curve-shaped cavity. *AIP Advances*, *11*(8), 085029. https://doi.org/10.1063/5.0061503.

Postelnicu, A. (2010). The effect of a horizontal pressure gradient on the onset of a Darcy–Bénard convection in thermal non-equilibrium conditions. *International Journal of Heat and Mass Transfer*, *53*(1-3), 68-75.

Sakshath, T.N., & P Joshi, A. (2021). Effect of horizontal pressure gradient on Rayleigh–Bénard convection of a Newtonian nanoliquid in a high porosity medium using a local thermal non-equilibrium model. *Heat Transfer*, *50*(2), 1631-1657.

Sarkar, J., Ghosh, P., & Adil, A. (2015). A review on hybrid nanofluids: recent research, development and applications. *Renewable and Sustainable Energy Reviews*, *43*, 164-77.

Sharma, J. (2024). Linear variations in conductivity and viscosity as particles' basic profile for convective instability in nanofluids under various boundary conditions. *Meccanica*, *59*(5), 729-742. https://doi.org/10.1007/s11012-024-01784-4.

Sharma, J., & Gupta, U. (2020). Nanofluid convection under Hall currents and LTNE effects. *Materials Today: Proceedings, 26*(3), 3369-3377.

Sharma, J., Gupta, U., & Wanchoo, R.K. (2016). Magneto binary nanofluid convection in porous medium. *International Journal of Chemical Engineering*, *2016*(1), 9424036. https://doi.org/10.1155/2016/9424036.

Sharma, J., Gupta, U., & Wanchoo, R.K. (2017). Numerical study on binary nanofluid convection in a rotating porous layer. *Differential Equations and Dynamical Systems*, *25*(2), 239-249.

Sheikholeslami, M., & Shehzad, S.A. (2018). Simulation of water-based nanofluid convective flow inside a porous enclosure via non-equilibrium model. *International Journal of Heat and Mass Transfer, 120*, 1200-1212.

Shilpee, & Bhadauria, B.S. (2023). Local thermal non-equilibrium and internal heating impact on thermal instability of Jeffrey nanofluid saturated porous media under different gravity modulations. *Journal of Nanofluids, 12*, 2092-2114.

Shilpee, & Bhadauria, B.S. (2024). Combined effect of local thermal nonequilibrium and gravity modulation on thermal instability in micropolar nanofluid saturated porous media. *Journal of Porous Media, 27*(2), 81-99.

Straughan, B. (2011). Tipping points in Cattaneo–Christov thermohaline convection. *Proceedings of the Royal Society A: Mathematical, Physical and Engineering Sciences*, *467*(2125), 7-18.

Suresh, S., Venkitaraj, K.P., Selvakumar, P., & Chandrasekar, M. (2011). Synthesis of Al2O3–Cu/water hybrid nanofluids using two step method and its thermo physical properties. *Colloids and Surfaces A: Physicochemical and Engineering Aspects*, *388*(1-3), 41-48.

Turcu, R., Darabont, A.L., Nan, A., Aldea, N., Macovei, D., Bica, D., & Biro, L. P. (2006). New polypyrrole-multiwall carbon nanotubes hybrid materials. *Journal of Optoelectronics and Advanced Materials*, *8*(2), 643-647.

Vadasz, P. (2006). Heat conduction in nanofluid suspensions. *Journal of Heat Transfer*, *128*(5), 465-477.

Ye, C., Li, B., & Sun, W. (2010). Quasi-steady-state and steady-state models for heat and moisture transport in textile assemblies. *Proceedings of the Royal Society A: Mathematical, Physical and Engineering Sciences*, *466*(2122), 2875-2896.